Jurnal Kejuruteraan 38(5) 2026: 2307-2315
https://doi.org/10.17576/jkukm-2026-38(5)-17

Solvent Debinding of Cu-Al-Ni Shape Memory Alloy Micro-Components Produced by Micro-Powder Injection Molding

Al Basir[a*], Norhamidi Muhamad[b], Abu Bakar Sulong[b], Kambiz Rashidi[b], Farhana Mohd Foudzi[b], Nabilah Afiqah Mohd Radzuan[b] & Nashrah Hani Jamadon[b]

[a]*Interdisciplinary Research Center for Advanced Materials, King Fahd University of Petroleum and Minerals, Dhahran 31261, Saudi Arabia*

[b]*Department of Mechanical and Manufacturing Engineering, Faculty of Engineering and Built Environment, Universiti Kebangsaan Malaysia, 43600 Bangi, Selangor, Malaysia*

Corresponding author: al.basir005@yahoo.com

Received 27 July 2025, Received in revised form 24 February 2026
Accepted 24 March 2026, Available online 30 August 2026

ABSTRACT

The escalating demand for the high-volume manufacturing of precisely detailed and small-scale parts has become increasingly pronounced over the past few years. In this context, micro-powder injection molding (µPIM), an advanced adaptation of the powder injection molding (PIM) technique, has proven to be a cost-effective and technically sophisticated method for the precise shaping and mass production of micro-scale metallic and ceramic parts. µPIM is a potentially efficacious process for the fabrication of micro-sized Cu-Al-Ni shape memory alloy (SMA) components. However, debinding remains challenging for micro-sized components, regardless of materials, because of their tendency toward cracking and dimensional distortion. This study involved the formulation of a 68 vol. % powder-loaded Cu-Al-Ni feedstock through the mixing of a Cu-Al-Ni powder mixture with a binder system, composed of paraffin wax (PW), high-density polyethylene (HDPE), and stearic acid (SA), at an elevated temperature of 150°C maintained for 1 hour period to ensure feedstock homogeneity. Green micro-components of Cu-Al-Ni SMA were produced through micro-injection molding by employing controlled process conditions comprising an injection pressure of 10 bar, an injection duration of 6 s, a mold temperature of 145°C, and a melt temperature of 180 °C. Following a solvent debinding procedure at 60°C for 1 hour, 74.4% of the PW and SA soluble binders were effectively removed from the green micro-component without inducing any defects or cracking in the component. The open channels formed in the solvent debound parts assist in the expulsion of the HDPE binder through thermal debinding phase.

Keywords: Shape memory alloy; Micro-powder injection molding; Cu-Al-Ni; Binder; Debinding

INTRODUCTION

A technologically sophisticated derivation of adaptive, functional materials referred to as shape memory alloys (SMAs) have an exceptional capacity to remember their previous shape prior to pseudoplastic deformation (Bouabdallah et al. 2013; Karagoz & Aksu Canbay 2013; Rashidi et al. 2024; Rashidi et al. 2025; Zare & Ketabchi 2016). The extraordinary behaviors of shape memory and superelasticity, definitive traits of SMAs, originate from a martensitic phase change that is both reversible in nature and governed by specific crystallographic rearrangements (Agrawal & Dube 2018; Ma et al. 2013). The properties of SMAs have made them useful across diverse fields, including robotics, actuators, automotive, aerospace, optoelectronics, construction, biomedical, and textile (Bil et al. 2018; Bendahan et al. 1997; Copaci et al. 2020; Canbay et al. 2016; Canbay & Karaduman 2021; Eschen et al. 2020; Hu et al. 2021; Jani et al. 2014; Kim et al. 2022; Long et al. 2022; Molod et al. 2022; Mwangi et al. 2019; Nespoli et al. 2022; Shakeriaski et al. 2022). Among the existing SMAs, Ni-Ti SMAs are quite renowned due to their high strain recovery and superior corrosion resistance (Alaneme & Okotete 2016; Dawood & Abid Ali 2022). The major challenge of Ni-Ti SMAs is their high production and materials costs (Alaneme et al. 2021; Muntasir Billah et al. 2022). Cu-based SMAs are advocated to be a compelling counterpart to Ni-Ti SMAs across various industries, owing to their cost-effectiveness (López et al. 2015; Saud et al. 2013). In recent times, Cu-Al-Ni SMAs are getting higher attention among researchers due to their excellent recoverable super-elastic strain, remarkable thermal stability, and outstanding damping capability (Suresh & Ramamurty 2008; Saud et al. 2015).

Powder injection molding (PIM) embodies a leading-edge technique indispensable for the nuanced fabrication of high-integrity components, encompassing an array of salient benefits, including negligible post-processing wastage, superior surface integrity, significant potential for miniaturization, unparalleled mechanical resilience, extensive material adaptability, and remarkable cost-effectiveness (Basir et al. 2023a; Basir et al. 2023b; Basir et al. 2022; Choi et al. 2017; Dehghan-Manshadi et al. 2018; Liu et al. 2005; Meng et al. 2011; Piotter et al. 2011; Wang et al. 2009). The PIM process incorporates several innovative variants, such as micro-PIM (µPIM) and co-macro/micro-PIM (2C-PIM/2C-µPIM) (Attia et al. 2014; Alcock 1999; Basir et al. 2024a; Basir et al. 2024b; Jung et al. 2015; Park et al. 2018). The µPIM technique is employed to manufacture small-scale components, which possess an outer measurement merely spanning several millimeters, in contrast to macro-scale parts, whose typical dimensions approach several tens of millimeters (Meng et al. 2011). Analogous to traditional PIM, µPIM facilitates the cost-efficient fabrication of micro-components composed of metals and ceramics. In recent times, there has been a marked surge in the demand for µPIM-manufactured micro-assemblies across sectors such as electronics, aerospace, biomedical engineering, and the automotive industry, attributed to their superior performance characteristics (Basir et al. 2021a; Basir et al. 2021b; Fu et al. 2004; Piotter et al. 2011; Tay et al. 2009). The fabrication of micro components through µPIM involves a sequence of four essential processes: the blending of materials, micro-injection molding, extraction of implemented binders, and sintering. A homogenous feedstock is achieved by amalgamating a finely dispersed powder with binders. The subsequent step involves the precise injection of this feedstock into a mold cavity, thereby forming a green micro-structure that conforms to the desired geometry. The debinding process, executed through a tailored technique, efficiently removes the binders from the molded entity. To achieve optimal densification and confer the requisite structural and functional properties, the debound micro-component is subjected to sintering (Meng et al. 2010; Wang et al. 2022).

Recently, researchers have focused on fabricating micro-sized Cu-Al-Ni SMA components utilizing the µPIM process; however, this approach remains inadequately investigated, particularly with respect to the debinding stage. Extracting the soluble binders from molded micro-scale SMA parts via the solvent debinding process poses considerable challenges, predominantly due to the susceptibility of the samples to crack formation and dimensional distortion. Despite these critical issues, systematic studies addressing the solvent debinding behavior of Cu-Al-Ni SMA micro-components produced by the µPIM approach are still limited. Therefore, the present research investigates the solvent debinding behavior of Cu-Al-Ni SMA micro-components fabricated via µPIM, thereby providing new insights into overcoming debinding-related defects at the micro-scale.

EXPERIMENTAL PROCEDURES

The present experimental framework incorporated Cu, Al, and Ni from Vistec Technology Services, Malaysia, with mean particle sizes of 52.1 µm, 11.9 µm, and 8.4 µm, respectively. Cu, Al, and Ni powders were mixed to prepare the powder mixture of 84Cu-12Al-4Ni (wt.%). Using a field emission scanning electron microscope (FESEM, Zeiss Merlin Compact), the powder mixture's morphology was examined and is shown in Figure 1. The pycnometer density of the Cu-Al-Ni powder mixture was 6.75 g/cm^3 and was measured by AccuPyc II 1340 Pycnometer.

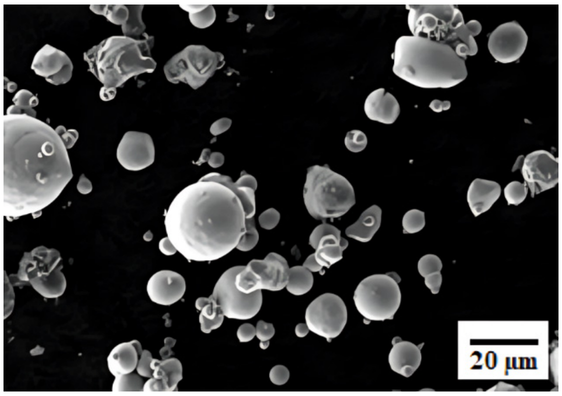

FIGURE 1. Morphology of powder mixture comprising Cu, Al, and Ni

Incorporation of paraffin wax (PW), high-density polyethylene (HDPE), and stearic acid (SA) binders was pivotal in the composition design. PW and SA were provided by Systerm Co. in Malaysia, whereas HDPE was acquired from Titanex, also based in Malaysia. The composition of PW, HDPE, and SA was 65 wt.%, 30 wt.%, and 5 wt.%, respectively. While the densities of the soluble binders PW and SA were 0.89 g/cm^3 and 0.98 g/cm^3, respectively, the density of the insoluble HDPE binder was 0.94 g/cm^3. PW enhanced the wettability and flowability characteristics of feedstock (Dehghan-Manshadi et al.

2017; Gal et al. 2019; Heaney et al. 2004; Li et al. 2009; Lu et al. 2011; Royer et al. 2015; Wang et al. 2016; Yi et al. 2017). HDPE was employed to strengthen the micro-sized green specimen (Aggarwal et al. 2006; Han et al. 2016). Moreover, the powder-binder contact angle was ameliorated by SA (Chuankrekkul et al. 2013; Kim et al. 2006; Li et al. 2007; Oh et al. 2018; Quinard et al. 2011; Qin et al. 2019; Supriadi et al. 2007; Sotomayor et al. 2010; Thavanayagam et al. 2015).

The Cu-Al-Ni feedstock was produced using a Brabender mixer (W50 EHT), in which 68 vol.% of Cu-Al-Ni metallic powder blend was mixed alongside PW, HDPE, and SA binders. The fabrication process was conducted under rigorously controlled parameters, ensuring blending at 150°C, an hour of processing duration, and blending at a speed of 25 rpm to ensure optimal dispersion and binder integration. A crusher was used to crush the resulting feedstock.

Defect-free green Cu-Al-Ni SMA micro-sized components were fabricated using a semiautomatic injection molding machine (DSM Xplore IM12), with optimized injection molding parameters. By diligently adhering to the optimal micro-injection molding conditions, it was ensured that the samples remained devoid of any imperfections, such as cracks, flashing, or short shots, thus preserving their structural integrity. The schematic of the Cu-Al-Ni micro-component is exhibited in Figure 2. Demolding was executed with rigorous precision following the completion of the molding, primarily to enable through mold cooling, to mitigate the risk of structural deformation of the specimen.

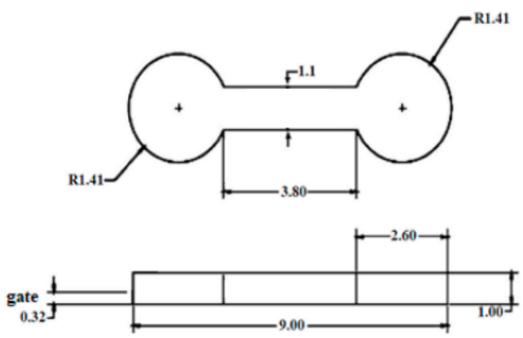

FIGURE 2. Schematic of micro-component (mm)

A drying oven (BINDER FDL 115) was used to carry out the solvent debinding process. The green Cu-Al-Ni micro-components underwent a 1-hour *n*-heptane immersion at 60°C to eradicate the PW and SA binders. The binder removal rate was evaluated by measuring mass loss in five micro-components under identical conditions. The rate at which the binder was extracted was ascertained through the utilization of the subsequent equation:

$$W_d(\%) = \frac{W_i - W}{W_i} \times 100 \tag{1}$$

Where W_d, W_i are W are the rate at which the binder is expelled, the primary weight of green micro-sized sample, and the weight of micro-sized sample subsequent to solvent debinding, respectively. The W_d value was divided by the overall binder percentage by weight contained in the initial material, thereby enabling the quantification of the cumulative binder mass expelled during the debinding process.

RESULTS AND DISCUSSION

The powder-binder integration, a step intricately shaped by a multitude of variables, marks the commencement of the μPIM. Among these, the thermal conditions and temporal extent of the mixing phase, the proportion of powder utilized, its size, the chronology of the introduction of components, and the shear rate exerted upon the blend, all exert significant influence on the ultimate quality of the feedstock. Subsequent stages of the process are incapable of rectifying any deficiencies in the inherent quality of the feedstock. In this investigation, a highly efficient dispersion of Cu-Al-Ni powder mixture within the soluble (PW and SA) and insoluble (HDPE) binders was realized with the aid of the employment of Brabender mixer throughout the blending process. Figure 3 illustrates the blending profile of the Cu-Al-Ni feedstock. The deployment of a mixer, which synchronized the quantification of mixing torque alongside the progression of process duration enabled a comprehensive assessment of Cu-Al-Ni feedstock's homogeneity. In conjunction with Figure 3, the homogeneity of the powder-binder mixture was firmly validated through the gradual stabilization of the value, which, subsequent to an early surge in the mixing torque, continued to persist consistently over the duration of the process. The formulation of a homogeneous feedstock is of paramount importance in optimizing the efficacy of any μPIM process. Beyond exacerbating the probability of fault development in a component, inhomogeneous feedstock exerts a deleterious influence on the mechanical properties, undermining the overall structural integrity and performance of the component (Supati et al. 2000). Figure 4 exhibits the FESEM image of the produced Cu-Al-Ni feedstock. As evidenced by Figure 4, the powder particles were entirely enveloped by the binder system, ensuring full coverage.

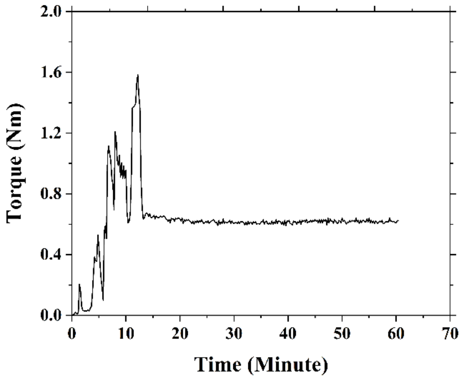

FIGURE 3. Mixing curve for Cu-Al-Ni feedstock

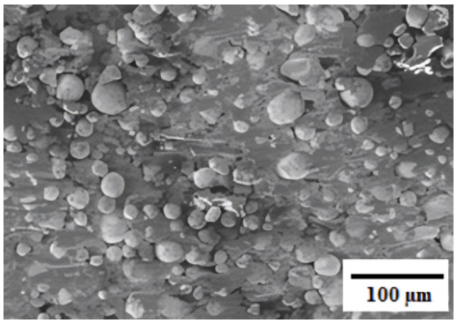

FIGURE 4. FESEM image of Cu-Al-Ni feedstock

Micro-injection molding experiments were executed on Cu-Al-Ni feedstock to facilitate the comprehensive elucidation and precise optimization of the requisite molding parameters. The parameters considered most compatible with the process specifications are outlined below:

1. Melt temperature: 180°C
2. Pressure applied during injection: 10 bar
3. Pressure during holding: 10 bar
4. Period of injection: 6 s
5. Mold temperature: 145°C

The study accentuated the paramount significance of mold temperature as a governing parameter in ensuring the dimensional exactitude and fabrication fidelity of micro-components fabricated via µPIM. It was discerned that a reduction in mold temperature below 145°C markedly precipitated the prevalence of short shot defects, thereby culminating in insufficient cavity fill and compromised component formation. This issue arose primarily as a result of the rapid cooling of the Cu-Al-Ni feedstock within the micro-injection molding process, which was intensified by the diminutive size of the mold cavity. Upon entering the mold, the feedstock underwent rapid thermal dissipation, leading to premature solidification that impeded its flowability. The reduced flowability caused by the feedstock's inability to maintain a sufficient molten state hindered its capacity to adequately fill the mold, thereby causing short shot defects (German & Bose 1997). In order to address this challenge, it became essential to attenuate the thermal disparity between the mold and the melt temperatures, ensuring that the molten feedstock retained sufficient fluidity throughout the injection process. By maintaining a more consistent temperature between the mold and the feedstock, the likelihood of premature solidification was significantly reduced, allowing for better mold filling and improved process reliability. Recent studies, such as those by Basir et al. (2023b) and Basir et al. (2024b), further support this approach, demonstrating that optimizing mold temperature not only mitigates short shot defects but also enhances part accuracy and consistency in the production of micro-scale components. Consequently, the optimal mold temperature of 145°C was identified as the key to ensuring the successful formation of defect-free green parts. This thermal setting enabled the Cu-Al-Ni feedstock to flow more efficiently, thereby enhancing the dimensional precision and structural integrity of the final components. This refined mold temperature control, therefore, serves as a crucial factor in achieving high-quality micro-injection molded components, emphasizing the importance of precise thermal management in advanced micro-fabrication techniques. A pressure of 10 bar was applied, as exceeding this threshold elevated the probability of flash defects occurring in the specimens. Figure 5 exhibits the green Cu-Al-Ni SMA micro-sized component. The FESEM image of the micro-injection molded Cu-Al-Ni micro-sized component is displayed in Figure 6. As presented in Figure 6, aside from the complete coating of powder particles by the binders, the micro-sample exhibited no detectable defects.

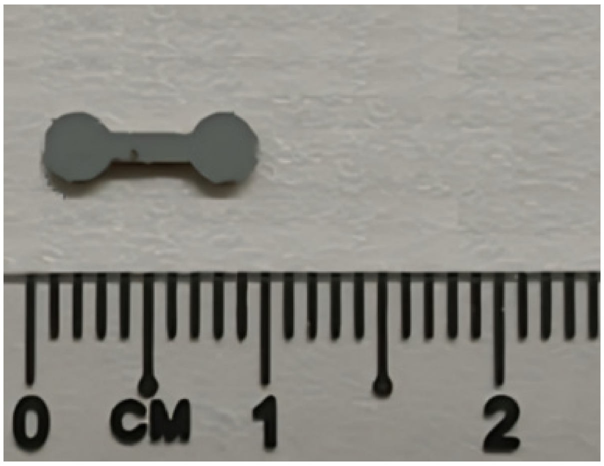

FIGURE 5. Green Cu-Al-Ni micro-component

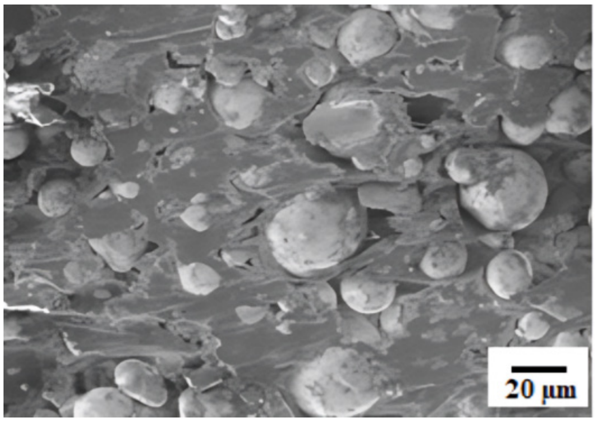

FIGURE 6. FESEM image of micro-injection molded Cu-Al-Ni part

Following the completion of the molding, the solvent debinding procedure was promptly undertaken to maintain process continuity. The intrinsic geometry of the green part, notably its surface-to-volume ratio, profoundly impacts the efficacy of the solvent debinding process, as it dictates the capacity of the solvent to penetrate the specimen's internal structure with precision, thereby enabling the thorough dissolution and extraction of the binder constituents. During the solvent debinding process in this study, the green-state micro-scale samples were submerged in the solvent, which induced PW and SA soluble binders to amalgamate with the solvent, resulting in the formation of a swelling gel. Once the solvent concentration attained a critical level, the gel began to dissolve. As the PW and SA binders were partially leached out, the micro-sized samples developed a porous morphology. With increasing debinding duration, these pores expanded, eventually infiltrating the interior of the sample (Hwang & Hsieh 1996; Sharmin & Schoegl 2014). The prevalence of structural imperfections, such as micro-cracks and large-scale defects, significantly escalates during the solvent debinding stage, primarily due to the considerable diminution in the mechanical robustness of the components following soluble binder removal, which leaves them acutely vulnerable to mechanical failure even under minimal external stresses. As reported by Basir et al. (2021b), earlier PIM and µPIM studies commonly used solvent debinding at 30–60°C to ensure efficient binder removal while minimizing dimensional distortion. While not governed by an explicit technical standard, this range has emerged as a practical benchmark, largely due to its effectiveness across diverse material systems and binder compositions. Building upon prior experimental insights, the current study executed solvent debinding at 60°C, intentionally selecting the upper limit of the commonly applied thermal range to enhance process efficacy. This choice ensured procedural continuity with earlier investigations while affording refined regulation of binder removal behavior. Operating at this temperature not only mitigated the risk of incomplete debinding but also preserved the dimensional fidelity and microstructural coherence of the component. Thus, the selected condition represented a judicious alignment with thermally optimized parameters that supported both reproducibility and material integrity throughout the mid phases of processing. Figure 7 delineates the time-dependent extraction of the PW and SA binders from the Cu-Al-Ni micro-component. According to Figure 7, the first 30 minutes were distinguished by a rapid expulsion of the soluble binder, after which the extraction rate significantly diminished over the following 30 minutes. After 1 hour, 74.4% of the PW and SA binders were eliminated from the micro-sized specimen. The solvent debinding process was intentionally confined to a duration of 1 hour, as experimental results revealed a marked decline in the efficiency of binder extraction after approximately 40 minutes of processing. This diminishing rate suggested that continued exposure to the solvent beyond this point would yield negligible benefits in terms of further binder removal. Furthermore, extending the debinding process beyond the 1-hour limit was associated with an increased likelihood of initiating structural degradation, including the propagation of microcracks and the development of other latent defects within the samples. Such imperfections could ultimately undermine the dimensional stability and mechanical integrity of the final components. The image depicting the defect-free solvent debound Cu-Al-Ni micro-component is presented in Figure 8. In contrast to the green body, no discernible structural alterations were detected in the solvent extracted body. Figure 9 illustrates the FESEM image of the solvent debound Cu-Al-Ni micro-component. As depicted in Figure 9, alongside the considerable removal of PW and SA, the specimen underwent the emergence of open porosity, an essential characteristic for facilitating the subsequent expulsion of the HDPE binder during the thermal debinding phase. A comprehensive investigation into the thermal debinding and sintering of Cu-Al-Ni SMA components produced via the µPIM will be pursued in a future study.

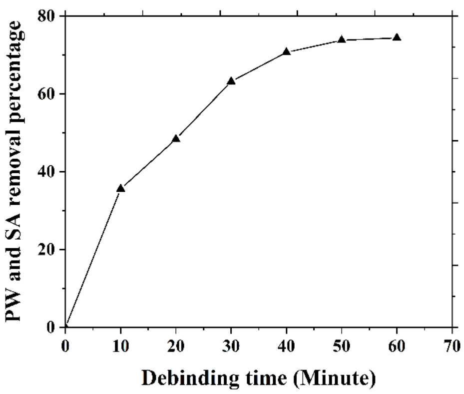

FIGURE 7. PW and SA elimination percentage at 60°C during solvent debinding

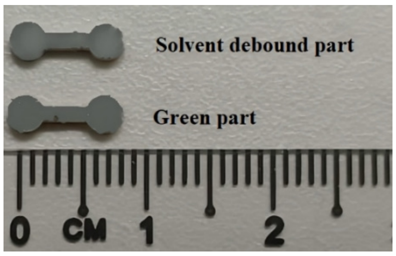

FIGURE 8. Green vs. solvent debound Cu-Al-Ni micro-component

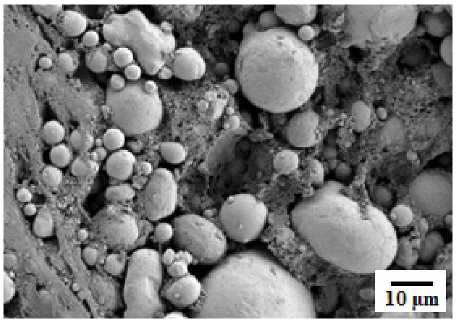

FIGURE 9. FESEM micrograph of solvent extracted Cu-Al-Ni micro-component

CONCLUSION

The feasibility of employing Cu-Al-Ni powder mixture to produce green SMA micro-sized components and their solvent extraction behavior was investigated in the present study. A Cu-Al-Ni feedstock containing 68 vol.% powder loading was fabricated through the mixing of a Cu-Al-Ni powder mixture with PW, HDPE, and SA binders at 150°C. The successful fabrication of structurally stable green Cu-Al-Ni micro-sized components was achieved, with the overall effectiveness of the injection molding process being primarily governed by the meticulous regulation of a critical parameter, namely the mold temperature, which plays an instrumental role in controlling the material flow dynamics and maintaining the consistency and structural cohesion of the molded components. Solvent extraction was executed at 60°C, resulting in the removal of 74.4% of PW and SA binders after a 1 hour immersion in a *n*-heptane, during which the majority of the soluble binder components were effectively extracted within the first 30 minutes. Furthermore, the complete absence of any defects within the solvent debound component serves as a definitive confirmation of the successful and precise execution of the solvent debinding process, thereby underscoring the efficacy of the procedure in ensuring the desired quality of the material. The thermal debinding and sintering behavior of the SMA micro-components will be investigated in a future study.

ACKNOWLEDGEMENT

The authors would like to thank Universiti Kebangsaan Malaysia for the financial support under the grant DIP-2024-020.

DECLARATION OF COMPETING INTEREST

None.

REFERENCES

Agrawal, A. & Dube, R. K. 2018. Methods of fabricating Cu-Al-Ni shape memory alloys. *Journal of Alloys and Compounds* 750: 235-247.

Alaneme, K. K. & Okotete, E. A. 2016. Reconciling viability and cost-effective shape memory alloy options–A review of copper and iron based shape memory metallic systems. *Engineering Science and Technology, an International Journal* 19(3): 1582-1592.

Alaneme, K. K., Anaele J. U., & Okotete, E. A. 2021. Martensite aging phenomena in Cu-based alloys: Effects on structural transformation, mechanical and shape memory properties: A critical review. *Scientific African* 12: e00760.

Attia, U. M., Hauata, M., Walton, I., Annicchiarico, D., & Alcock, J. R. 2014. Creating movable interfaces by micro-powder injection moulding. *Journal of Materials Processing Technology* 214 (2): 295–303.

Alcock, J. 1999. Co-injection promises further growth for MIM. *Metal Powder Report* 54(6): 30-34.

Aggarwal, G., Park, S. J., & Smid, I. 2006. Development of niobium powder injection molding: Part I. Feedstock and injection molding. *International Journal of Refractory Metals and Hard Materials* 24 (3): 253-262.

Bouabdallah, M., Baguenane-Benelia, G., Saadi, A., Cheniti, H., Gachon, J. C., & Patoor, E. 2013. Precipitation sequence during ageing in β_1 phase of Cu–Al–Ni shape memory alloy. *Journal of Thermal Analysis and Calorimetry* 112: 279-283.

Bil, C., Massey, K., & Abdullah E. J. 2013. Wing morphing control with shape memory alloy actuators. *Journal of Intelligent Material Systems and Structures* 24(7): 879-898.

Bendahan, M., Seguin, J. L., Lollman, D., & Carchano, H. 1997. New type of Schottky barriers using NiTi shape memory alloy films. *Thin Solid Films* 294(1-2):278-280.

Basir, A., Muhamad, N., Sulong, A. B., Jamadon, N. H., & Foudzi, F. M. 2023a. Recent Advances in Processing of Titanium and Titanium Alloys through Metal Injection Molding for Biomedical Applications: 2013–2022. *Materials* 16 (11): 3991.

Basir, A., Muhamad, N., Sulong, A. B., Amin, M. M., Jamadon, N. H., & Radzuan, N. A. M. 2023b. Micro-injection molding and debinding behavior of hydroxyapatite/ zirconia bi-materials fabricated by two-component micro-powder injection molding process. *Materials* 16 (19): 6375.

Basir, A., Sulong, A. B., Jamadon, N, H., & Muhamad, N. 2022. Physical Properties of Sintered Stainless Steel 17-4PH Micro-Part Processed by MicroPowder Injection Molding. *Jurnal Kejuruteraan* 34(6): 1209-1214.

Basir, A., Sulong, A. B., Muhamad, N., Juri, A. Z., Jamadon, N. H, Foudzi, F. M., Radzuan, N. A. M., & Rashidi, K. 2024a. Influence of SS316L nanoparticles on the sintered properties of two-component micro-powder injection moulded bimodal SS316L/zirconia bi-materials. *Materials* 17 (22): 5536.

Basir, A., Sulong, A. B., Muhamad, N., Juri, A. Z., Jamadon, N. H, Foudzi, F. M., & Radzuan, N. A. M. 2024b. Debinding of Yttria-Stabilised Zirconia/ Bimodal Stainless Steel 316L Bi-Materials Produced through Two-Component Micro-Powder Injection Moulding. *Polymers* 16 (13): 1831.

Basir, A., Sulong, A. B., Jamadon, N. H., & Muhamad, N. 2021a. Feedstock properties and debinding mechanism of yttria-stabilized zirconia/ stainless steel 17-4PH micro-components fabricated via two-component micro-powder injection molding process. *Ceramics International* 47 (14): 20476-20485.

Basir, A., Sulong, A. B., Jamadon, N. H., Muhamad, N., & Emeka U. B. 2021b. Process parameters used in macro/micro powder injection molding: An overview. *Metals and Materials International* 27: 2023-2045.

Copaci, D. S., Blanco, D., Martin-Clemente, A., & Moreno, L. 2020. Flexible shape memory alloy actuators for soft robotics: modelling and control. *International Journal of Advanced Robotic Systems* 17: 1-15.

Canbay, C. A., Tataroglu, A., Dere, A., Al-Ghamdi, A., & Yakuphanoglu, F. 2016. A new shape memory alloy film/p-Si solar light four quadrant detector for solar tracking applications. *Journal of Alloys and Compounds* 688:762–768.

Canbay, C. A. & Karaduman, O. 2021. The photo response properties of shape memory alloy thin film based photodiode. *Journal of Molecular Structure* 1235: 130263.

Choi, J. P., Park, J. S., Hong, E. J., Lee, W. S., & Lee, J. S. 2017. Analysis of the rheological behavior of Fe trimodal micro-nano powder feedstock in micro powder injection molding. *Powder Technology* 319: 253-260.

Chuankrekkul, N., Boonyongmaneerat, Y., Saengkiettiyut, K., Rattanawaleedirojn, P., & Saenapitak, S. 2013. Injection moulding of tungsten carbide-nickel powders prepared by electroless deposition. *Key Engineering Materials* 545: 158-152.

Dawood, N. M. & Abid Ali, A. R. 2022. Effect of aging on corrosion behavior of martensite phase in Cu-Al-Ni shape memory alloy. *Key Engineering Materials* 911: 96-102.

Dehghan-Manshadi, A., StJohn, D., Dargusch, M., Chen, Y., Sun, J.F., & Qian, M. 2018. Metal injection moulding of non-spherical titanium powders: Processing, microstructure and mechanical properties. *Journal of Manufacturing Processes* 31: 416–423.

Dehghan-Manshadi, A., Bermingham, MJ., Dargusch, M. S., StJohn, D. H., & Qian, M. 2017. Metal injection moulding of titanium and titanium alloys: Challenges and recent development. *Powder Technology* 319: 289-301.

Eschen, K., Granberry, R., & Abel, J. 2020. Guidelines on the design, characterization, and operation of shape memory alloy knitted actuators. *Smart Materials and Structures* 29: 035036.

Fu, G., Loh, N. H., Tor, S. B., Murakoshi, Y., & Maeda, R. 2004. Replication of metal microstructures by micro powder inection molding. *Materials & Design* 25(8): 729-733.

Gal, C. W., Song, G. W., Baek, W. H., Kim, H. K., Lee, D. K., Lim, K. W., & Park, S. J. 2019. Fabrication of pressureless sintered Si_3N_4 ceramic balls by powder injection molding. *Ceramics International* 45 (5): 6418-6424.

German, R, M. & Bose, A. 1997. Injection Molding of Metals and Ceramics. Princeton, NJ, USA: Metal Powder Industries Federation

Hu, K., Rabenorosoa, K., & Ouisse, M. 2021. A review of SMA-based actuators for bidirectional rotational motion: application to origami robots. *Frontiers in Robotics and AI* 8: 678486.

Heaney, D. F., Zauner, R., Binet, C., Cowan, K., & Piemme, J. 2004. Variability of powder characteristics and their effect on dimensional variability of powder injection moulded components. *Powder Metallurgy* 47 (2): 144-149.

Han, J. S., Gal, C. W., Kim, J. H., & Park, S. J. 2016. Fabrication of high-aspect-ratio micro piezoelectric array by powder injection molding. *Ceramics International* 42 (8): 9475-9481.

Hwang, K. S. & Hsieh, Y.M. 1996. Comparative study of pore structure evolution during solvent and thermal debinding of powder injection molded parts. *Metallurgical and Materials Transactions A* 27: 245-253.

Jani, J. M., Leary, M., Subic, A., & Gibson, M. A. 2014. A review of shape memory alloy research, applications and opportunities. *Materials & Design* 56:1078–1113.

Jung, I. D., Park, J. M., Kang, T. G., Kim, S. J., & Park, S. J. 2015. Magneto-rheological model for computational analysis of magnetic micro powder injection molding. *Computational Materials Science* 100: 39–44.

Karagoz, Z. & Aksu Canbay, C. 2013. Relationship between transformation temperatures and alloying elements in Cu–Al–Ni shape memory alloys. *Journal of Thermal Analysis and Calorimetry* 114: 1069-1074.

Kim, M. S., Lee, H. S., Cho, Y., Heo, J. K., Quan, Y. J., Lee, S. W., Pahk, H. J., & Ahn, S. H. 2022 Surface nanopatterned shape memory alloy (SMA)-Based photosensitive artificial muscle. *Advanced Optical Materials* 10: 2102024.

Kim, S. W., Suk, M. J., & Kim, Y. D. 2006. Metal injection molding of W-Cu powders prepared by low energy ball milling. *Metals and Materials International* 12: 39-44.

Long, F., Cheng, Y., Ren, Y., Wang, J., Li, Z., Sun, A., & Xu, G. 2022. Latest advances in development of smart phase change material for soft actuators. *Advanced Engineering Materials* 24: 2100863.

López, G., López-Ferreño, I., Kilmametov, A. R., Breczewski, T., Straumal, B. B., Baretzky, B., Nó, M. L., & San Juan, J. 2015. Severe plastic deformation on powder metallurgy Cu–Al–Ni shape memory alloys. *Materials Today: Proceedings* 2: S747-S750.

Liu, L., Loh, N. H., Tay, B. Y., S. B., Murakoshi, Y., & Maeda, R. 2005. Mixing and characterisation of 316L stainless steel feedstock for micro powder injection molding. *Materials Characterization* 54: 230-238.

Li, D., Hou, H., Tan, Z., & Lee, K. 2009. Metal injection molding of pure molybdenum. *Advanced Powder Technology* 20 (5): 480-487.

Lu, Z., Zhang, K., & Wang, C. 2011. Effects of oxidation on the strength of debound SiC parts by powder injection moulding. *Powder Technology* 208: 49-53.

Li, Y., Li, L., & Khalil,K. A. 2007. Effect of powder loading on metal injection molding stainless steels. Journal of Materials Processing Technology 183 (2-3): 432-439.

Ma, J., Karaman, I., & Noebe, R.D. 2013. High temperature shape memory alloys. *International Materials Reviews* 55: 257-315.

Molod, M. A., Spyridis, P., & Barthold, F. J. 2022. Applications of shape memory alloys in structural engineering with a focus on concrete construction–A comprehensive review. *Construction and Building Materials* 337: 127565.

Mwangi, J.W., Nguyen, L.T., Bui, V.D., Berger, T., Zeidler, H., & Schubert, A. 2019. Nitinol manufacturing and micromachining: A review of processes and their suitability in processing medical-grade nitinol. *Journal of Manufacturing Processes* 38: 355-369.

Muntasir Billah, A. H. M., Rahman, J., & Zhang, Q. 2022. Shape memory alloys (SMAs) for resilient bridges: A stateof-the-art review. *Structures* 37: 514-527.

Meng, J., Loh, N. H., Fu, G., Tay, B. Y., Tor, & S. B. 2011. Micro powder injection moulding of alumina micro-channel part. *Journal of the European Ceramic Society* 31: 1049-1056.

Meng, J., Loh, N. H., Fu, G., Tor, S. B., & Tay, B. Y. 2010. Replication and characterization of 316L stainless steel micro-mixer by micro powder injection molding. Journal of Alloys and Compounds 496(1–2): 293-299.

Nespoli, A., Passaretti, F., Szentmiklosi, L., Maroti, B., Placidi, E., Cassetta, M., Yada, R. Y., Farrar, D. H., & Tian, K. V. 2022. Biomedical NiTi and β-Ti alloys: From composition, microstructure and thermomechanics to application. *Metals* 12(3): 406.

Oh, J. W., Seong, Y., & Park, S. J. 2018. Effects of nanoparticle in bimodal powder on physial and mechanical properties of powder injection molded parts. *Journal of Materials Processing Technology* 262: 503-510.

Piotter, V., Bauer, W., Knitter, R., Mueller, M., Mueller, T., & Plewa, K. 2011. Powder injection moulding of metallic and ceramic micro parts. *Microsystem Technologies* 17: 251-263.

Park, J. M., Han, J. S., Gal, C. W., Oh, J. W., Kim, J. H., Kate, K. H., Atre, S. V., Kim, Y., & Park, S. J. 2018. Fabrication of micro-sized piezoelectric structure using powder injection molding with separated mold system. *Ceramics International* 44(11): 12709-12716.

Quinard, C., Song, J., Barriere, T., & Gelin, J. C. 2011. Elaboration of PIM feedstocks with 316L fine stainless steel powders for the processing of micro-components. *Powder Technology* 208: 383-389.

Qin, M., Lu, H., Wu, H., He, Q., Liu, C., X., Wang, Y., Jia, B., & Qu, X. 2019. Powder injection molding of complex-shaped aluminium nitride ceramic with high thermal conductivity. *Journal of the European Ceramic Society* 39 (4): 952-956.

Rashidi, K., Sulong, A. B., Muhamad, N., Fayyaz, A., Foudzi, F. M., & Basir, A. 2024. Martensitic transformation characteristics, mechanical properties and damping behavior of Cu–Al–Ni shape memory alloys: A review of their modifications and improvements. *Journal of Materials Research and Technology* 29: 2732-2749.

Rashidi, K., Sulong, A. B., Muhamad, N., Fayyaz, A., Foudzi, F. M., & Basir, A. 2025. Microstructural evolution of Cu-Al-Ni shape memory alloys fabricated by powder injection molding. *Journal of the Japan Society of Powder and Powder Metallurgy* 72: S613-S616.

Royer, A., Barriere, T., & Gelin, J. C. 2015. The degradation of poly(ethylene glycol) in an Inconel 718 feedstock in the metal injection moulding process. *Powder Technology* 284: 467-474.

Shakeriaski, F., Ghodrat, M., Rashidi, M., & Samali, B. 2022. Smart coating in protective clothing for firefighters: an overview and recent improvements. *Journal of Industrial Textiles* 51(5S): 7428S-7454S.

Saud, S. N., Hamzah, E., Abubakar, T., & Hosseinian, R. 2013. A review on influence of alloying elements on the microstructure and mechanical properties of Cu-Al-Ni shape memory alloys. *Jurnal Teknologi* **6**4: 51-56.

Suresh, N. & Ramamurty, U. 2008. Aging response and its effect on the functional properties of Cu–Al–Ni shape memory alloys. *Journal of Alloys and Compounds* 449(1-2): 113-118.

Saud, S. N., Hamzah, E., Abubakar, T., Ibrahim, M. K., & Bahador, A. 2015. Effect of a fourth alloying element on the microstructure and mechanical properties of Cu–Al–Ni shape memory alloys. *Journal of Materials Research* 30(14): 2258-2269.

Supriadi, S., Baek, E. R., Choi, C. J., & Lee, B. T. 2007. Binder system for STS 316 nanopowder feedstocks in micro-metal injection molding. *Journal of Materials Processing Technology* 187-188: 270-273.

Sotomayor, M. E., Várez, A., & Levenfeld, B. 2010. Influence of powder particle size distribution on rheological properties of 316L powder injection moulding feedstocks. *Powder Technology* 200: 30-36.

Supati, R., Khor, K. A. & Tor, S. B. 2000. Mixing and characterization of feedstock for powder injection molding. *Materials Letters* 46(2–3): 109-114.

Sharmin, K. & Schoegl, I. 2014. Optimization of binder removal for ceramic microfabrication via polymer co-extrusion. *Ceramics International* 40: 3939-3946.

Tay, B. Y., Loh, N.H., Tor, S. B., Ng, F. L., Fu, G., & Lu, X. H. 2009. Characterisation of micro gears produced by micro powder injection moulding. *Powder Technology* 188(3): 179-182.

Thavanayagam, G., Pickering, K. L., Swan, J. E., & Cao, P. 2015. Analysis of rheological behaviour of titanium feedstocks formulated with a water-soluble binder system for powder injection moulding. *Powder Technology* 269: 227-232.

Wang, Q., Yin, H., Qu, X., & Johnson, J. L. 2009. Effects of mold dimensions on rheological of feedstock in micro powder injection molding, Powder Technology 193: 15-19.

Wang, C., Li, Z., Tian, W., Li, Y., Tang, L., Pang, Q., & Chen, M. 2022. Micro powder injection molding of boron carbide components with SiC-Al_2O_3-Y_2O_3 sintering additives. *Chinese Journal of Aeronautics* 35(5): 429-440.

Wang, W., Song, J., Yan, B., & Yu, Y. 2016. Metal injection molding of tungsten and its alloys. *Metal Powder Report* 71 (6): 441-444.

Yi, Y., Liang, Q., Jingwu, Z., Yao, Y., Wangchang, L., Jing, Y., Shenglei, C., & Liqiang, J. 2017. Effect of microcrystalline wax on the solvent debinding of the Sr-ferrite ceramics prepared by powder injection molding. *Journal of the European Ceramic Society* 37 (5): 2105-2114.

Zare, M. & Ketabchi, M. 2016. Effect of chromium element on transformation, mechanical and corrosion behavior of thermomechanically induced Cu–Al–Ni shape-memory alloys. *Journal of Thermal Analysis and Calorimetry* 127(3): 2113-2123.